



NS1 glycoprotein detection in serum and urine as an electrochemical screening immunosensor for dengue and Zika virus

Priscila D. Mendonça¹ · Lorena K. B. Santos¹ · Marcos V. Foguel¹ · Marco A. B. Rodrigues² · Marli T. Cordeiro³ · Luís M. Gonçalves⁴ · Ernesto T. A. Marques⁵ · Rosa F. Dutra¹ 

Received: 25 March 2021 / Revised: 21 May 2021 / Accepted: 31 May 2021 / Published online: 21 June 2021
© Springer-Verlag GmbH Germany, part of Springer Nature 2021

Abstract

The incidence of infection by the dengue virus (DENV) has grown dramatically, reaching 128 countries in tropical and subtropical regions worldwide, with a pattern of hyper-endemicity. DENV is a mosquito-borne disease having four serotypes, one or two circulating in epidemic outbreaks. The diagnosis of DENV is challenging mainly due to the circulation of new viruses with remarkable similarities, such as Zika (ZIKV) that may cause fetal microcephaly. DENV affects 390 million people per year, but these numbers may be higher due to the underreported and misclassified cases. Recently, the NS1 nonstructural protein has been described in serum and urine of DENV and ZIKV patients, suggesting its use as a biomarker for screening since a negative NS1 sample confirms the absence of these infections. Herein, a label-free immunosensor comprising an assembled nanostructured thin film of carbon nanotube-ethylenediamine is described. The advantage of in situ electrosynthesis of polymer film is to allow major control of thickness and conductivity, in addition to designing the reactive groups for functionalization. A quartz crystal microbalance system was used to estimate the thickness of the polymeric film obtained. The anti-NS1 monoclonal antibodies were immobilized to carbon nanotubes by covalent linkage, permitting a high stability during measurements. Analytical responses to NS1 were obtained by differential pulse voltammetry (DPV), showing a linear range from 20 to 800 ng mL⁻¹ and reproducibility of 3.0%, with a limit of detection (LOD) of 6.8 ng mL⁻¹. This immunosensor was capable of detecting ZIKV and DENV NS1 in spiked urine and real serum in a clinical range.

Keywords Immunosensor · Label-free · NS1 · Dengue virus · Zika virus

Introduction

Dengue is one of the oldest arboviruses globally, endemic in tropical and subtropical regions, transmitted mainly by the *Aedes aegypti* mosquitoes and affects more than 125 countries [1]. Severe forms can lead to hemorrhagic fever or dengue shock resulting in death [2]. It is estimated 390 million individuals are infected per year; however, the number of cases fluctuates according to the seasonality of the disease [3]. There is no specific vaccine or therapy, and prevention by massive testing of mosquitoes and infected individuals is one of the strategies for controlling the disease. The gold-standard diagnostic test for DENV is the polymerase chain reaction (PCR) that detects the viral RNA. However, it is prohibitively expensive, mainly in epidemic outbreaks, besides requiring complicated procedures in amplification to avoid contamination and care in sample collection. Cost-

✉ Rosa F. Dutra
rosa.dutra@ufpe.br

¹ Biomedical Engineering Laboratory, Federal University of Pernambuco, Recife, PE 50670-901, Brazil

² Electronic Department, Federal University of Pernambuco, Recife, PE 50740-550, Brazil

³ Department of Virology and Experimental Therapy, Oswaldo Cruz Foundation – FIOCRUZ, Aggeu Magalhães Institute, Recife, PE 50670-420, Brazil

⁴ Institute of Chemistry, University of São Paulo, São Paulo, SP 5508-000, Brazil

⁵ Department of Infectious Diseases and Microbiology, University of Pittsburgh, Center for Vaccine Research, Pittsburgh, PA 15261, USA

effective tests based on immunoassay are urgently needed to detect DENV more quickly and efficiently. The NS1 non-structural secretory protein has been considered a powerful marker of DENV, and several immunochromatographic rapid tests have been developed in the last decade [4]. In the acute phase of viral replications, there is a significant increase in NS1 concentrations in the bloodstream [5, 6].

Although some studies have found the NS1 protein only in individuals infected with DENV, this description is not a consensus. ZIKV is closely related to DENV, and during the acute phase of disease, the Zika virus might release NS1 protein into the bloodstream [7, 8]. Besides, ZIKV infection has apparent symptoms very similar to DENV; it is most severe in pregnant being associated with severe congenital microcephaly and malformations in infants [9, 10]. The same mosquitoes of DENV transmit ZIKV; however, given the ZIKV ability to infect the reproductive tract [11], it may also be transmitted via sexual intercourse [12, 13]. There is no controversy regarding the presence of Zika virus RNA in urine [7]. ZIKV RNA can be identified in urine and in whole blood for a longer period; however, a negative result does not rule out infection even early after symptom onset. In many countries endemic for DENV, co-infection with DENV and ZIKV occurs, meaning that the NS1 serological tests for differential diagnosis are not exhaustive, requiring the molecular PCR test. However, there is a consensus that the absence of NS1 protein precludes a positive diagnosis for DENV and ZIKV. DENV-NS1 in urine has been reported and also in saliva [8]. Urine offers obvious advantages for sample collection in groups as newborns and patients.

Given the great importance of NS1, many immunosensors for NS1 protein detection have been proposed using different transducers, including optical detection based on localized surface plasmon resonance [14], fluorescence [15], impedimetric [16], amperometric [17] and others. Nevertheless, among them, label-free electrochemical transducers are a more attractive alternative, due to the possibility of easy portability, which can result in a quick point-of-care diagnosis such as with the use of glucometers [18].

In electrochemical biosensors, the use of conductive polymer associated with carbon nanomaterials has been shown as an attractive strategy to obtain nanocomposites with high chemical stability and conductivity [19, 20]. Polymers derived from pyrrol and thiophene have been used alone as well in combination with carbon nanotubes [21, 22]. The way that nanocomposites are synthesized on the electrode surface is crucial, because it can affect the electrochemical properties and conductivity by effects on the electron transfer and charge net. Conventional methods for synthesis such as drop-casting and dip-coating have produced films with uncontrolled thickness, irregularities on the surface and several pinholes [23]. When polymer films are obtained by electrosynthesis, it

is possible to control the thickness in nanoscale, based on the electrochemical technique, number of cycles of cyclic voltammetry (CV), pH and other factors. Amine-rich conducting polymers seem more advantageous for biosensors than simply conducting polymers, because they are readily functionalized for linking to biomolecules by carboxylic groups, or to the carbon nanostructures [24].

In this study, we designed the development of an immunosensor for NS1 glycoprotein combining a carboxylated multi-walled carbon nanotube (CNT-COOH) and thin and short-branched poly-ethylenediamine (poly-EDA) forming a high-conductivity film to detect NS1 in serum and urine samples in a range of clinical levels.

Materials and methods

Reagents and materials

Ethylenediamine (EDA, 98%), ethyldimethylamine-propyl carbodiimide (EDC), hydroxysuccinimide (NHS), glycine, potassium ferricyanide ($K_3[Fe(CN)_6]$) and potassium ferri-cyanide [$K_3Fe(CN)_6$] were obtained from Sigma-Aldrich (St. Louis, MO, USA). Multi-walled carbon nanotubes functionalized with carboxylic acid (CNT-COOH, > 8% functionalized) were purchased from Dropsens (Oviedo, Spain). Anti-NS1 antibodies and NS1 protein were acquired from Abcam (Cambridge, UK). Phosphate-buffered saline (PBS) (0.01 mol L^{-1} , pH 7.4) was used in all experiments for dilution of the samples. Ultrapure water obtained from a Millipore water purification system (18 M Ω , Milli-Q, Millipore) was used in all experiments. All other chemicals used were of analytical grade.

Pools of spiked sera used in the study were prepared from a mixture of five sera from healthy individuals collected by venipuncture. The blood was collected in a dry tube and centrifuged at 15,000 RPM for 10 min. Lipemic serum was discarded to prepare pools spiked with NS1 at the desired concentration for analysis. The urine samples used in this study were collected in a clean dry tube, free of preservatives, from two healthy volunteers and were also spiked with NS1 in the desired concentration for the test.

In addition to the spiked samples, samples from ZIKV-infected individuals confirmed by molecular diagnosis via RT-PCR and IgM ELISA with assay protocol according to the Centers for Disease Control and Prevention (CDC) from the USA were also used in this study. Sera with a positive diagnosis of DENV was confirmed by protocols already described, in addition to the cultivation of the virus. For this study, sera from positive ZIKV individuals who had also been previously co-infected with DENV were discarded, which was very common in the study, because the ZIKV sample collection zone was endemic for DENV. The positive ZIKV

individuals were admitted to the Hospital das Clínicas Universitário in Recife, Pernambuco, the Brazilian state most affected during the ZIKV outbreak in 2016. All samples used in this study were from volunteers who signed informed consent forms, and the required protocols were approved by the Ethics Committee of the CPqAM/FIOCRUZ (protocol number 28309414.9.0000.5190).

Electrochemical and piezoelectric measurements

Electrochemical measurements were carried out by the Ivium CompactStat potentiostat (Eindhoven, Netherlands) interfaced with a computer, and software controlled by IviumSoft. It was used a conventional three-electrode system, comprising a gold electrode (EAu) as the working electrode (area of 0.985 mm²), Ag/AgCl in saturated KCl (Ag/AgCl, KCl_{sat}) as the reference electrode and platinum wire (Pt) as the counter electrode. The electrodes were immersed in a 5 mL electrochemical cell with 5 mmol L⁻¹ K₄ [Fe(CN)₆]⁴⁻/K₃ [Fe(CN)₆]³⁻ in KCl solution at 0.1 mol L⁻¹ measured at room temperature (approximately 23 °C).

Modifications that occurred on the electrode surface were characterized by cyclic voltammetry (CV) with a potential window from -0.2 to 0.6 V at 50 mV s⁻¹ and pretreatment of 10 s for stabilization of the residual current. Analytical measurements were performed using differential pulse voltammetry (DPV), applying a modulation amplitude of 25 mV, modulation time of 50 ms and interval time of 500 ms, with a step potential of 5 mV s⁻¹. The analytical responses of NS1 were obtained from the differential currents of the anodic peaks discounting the blank (ΔI), the ready electrode before the NS1 incubations.

Changes in the sensor surface were also characterized by a piezoelectric quartz crystal microbalance (QCM) system. The QCM system consisted of a 10 MHz quartz crystal electrode (Universal Sensors, USA) coupled to a home-made oscillator circuit that was developed by our group [25]. The oscillating circuit was designed to operate with two crystal electrodes, one reference whose oscillating frequency was adjusted to zero to match the difference between them. These initial calibrations are essential for restoring the equilibrium and make possible the comparisons among QCM electrodes since their resonance frequency can be slightly discrepant. Here, only one crystal electrode was modified. The QCM system was programmed to operate in a continuous flow mode at a rate of 100 μ L/min supplied by a peristaltic pump (Watson-Marlow SCI Q 400 model, UK). During each step of the crystal electrode modifications, measurements were recorded by a frequency counter (Agilent - model 011, USA). During measurements, the flow was turned off, avoiding fluctuation on the baseline.

Chemical and morphological characterization

FTIR in attenuated total reflectance (ATR) spectra provided information on functional groups near the surface ($\sim 1 \mu$ m) of internal reflection elements. To obtain spectra in ATR mode, a compact Bruker ALPHA IFS 66e⁻ spectrometer (Germany) was used in the range of 500 to 4000 cm⁻¹ with 20 scans.

For morphological characterizations, micrographs were obtained by scanning electron microscopy (SEM) using a TESCAN VEGA3 microscope with LM-type compartment and tungsten filament with secondary electron and backscattered electron detectors. To obtain the images, the gold discs were metalized over a period of 180 s using a Quorum Technologies Ltd. Q15OR modular coating system (Ashford, UK).

Growth of nanostructured polymer film on the sensor surface

The polymer film was obtained from EDA monomers using the CV electrochemical technique. For electropolymerization, the three electrodes were immersed in an electrochemical cell with an internal volume of 5 mL containing a mixture of 0.1 mol L⁻¹ EDA and 0.1 mol L⁻¹ of lithium perchlorate prepared in acetonitrile. Polymerization was carried out at a scan rate of 50 mV s⁻¹ in a potential window between -1.8 and 1.9 V with a step potential of 10 mV during 25 cycles.

Afterward, the CNT-COOH was covalently linked to the poly-EDA film. Prior to use, 1 mg of CNT-COOH was dispersed in 1 ml of dimethylformamide (DMF) and subjected to an ultrasound bath at 40 kHz for 1 h. After dispersion, CNT-COOH was pre-activated by incubating with EDC (40 mol L⁻¹) and NHS (100 mol L⁻¹) prepared in 0.1 mol L⁻¹ of acetate buffer (pH 5.5) and left to stand for 1 h at room temperature (~ 24 °C). Then, an aliquot (5 μ L) of the pre-activated CNT-COOH was pipetted on the electrode surface and left to react for 1 h, followed by two washes with PBS.

To perform the piezoelectric measurements, instead of using the gold electrode as described, the crystal electrode (Universal Sensors, USA) was employed as the working electrode with both terminals short-circuited, using the mentioned reference and counter electrodes immersed in a 5-mL cell, with the same electrochemical parameters for electropolymerization.

Immobilization of the anti-NS1 antibodies and immunoassay

Immobilization of the anti-NS1 antibody was performed by pipetting an aliquot (2 μ L) of anti-NS1 (10 μ g mL⁻¹) on the electrode surface [26]. The electrode was incubated in a moist chamber for 1 h at room temperature (~ 24 °C). The remaining

non-covalently bound antibodies were removed with five washes with PBS for 2 min each, followed by rinsing with ultrapure water. The remaining free reactive carboxylic groups were blocked with 50 mmol L⁻¹ glycine prepared in 0.1 mol L⁻¹ of citrate phosphate buffer (pH 5.5).

Analytical responses were obtained by incubating the electrode surface with 2 μL of samples for 30 min followed by placement in a moist chamber at 37 °C. Samples of serum and urine were diluted with 10 mM PBS (pH 7.4) for further analyses.

Results and discussion

Electrosynthesis of the poly-EDA/CNT-COOH film

Figure 1 exhibits a typical cyclic voltammogram of the electrochemical growth of polymer film on the electrode surface. EDA monomers were electrochemically oxidized to a peak of approximately 0.88 V. The first oxidation peak can be attributed to oxidation of an amino group that corresponds to the radical NH₂⁺ cation. The reduction currents in oxidation peaks are due to the binding of the EDA monomers on the electrode surface. Also observed was an increase in the reduction current, showing that radical cations were consumed during the electropolymerization of the poly-EDA, as well as different amine polymers [24, 27, 28].

The current density supplied for electropolymerization affects the thickness and conductivity of the film. Figure S1a (see Supplementary Information, ESM) shows the profile of

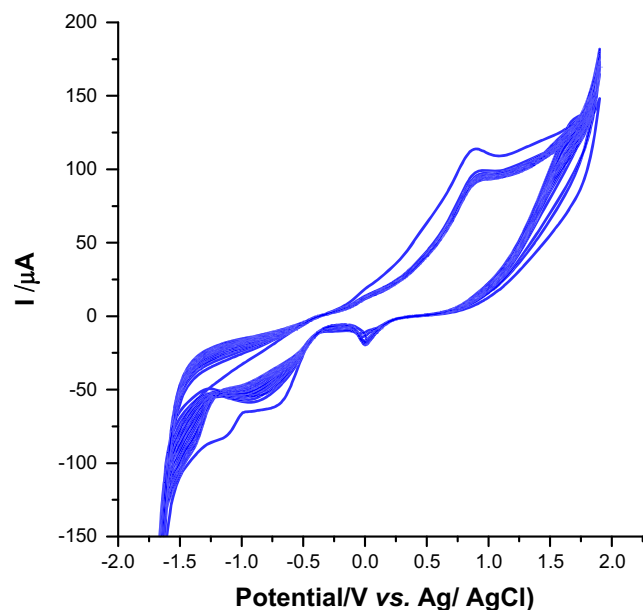


Fig. 1 Typical cyclic voltammogram of the electrosynthesis of the poly-EDA by 25 cycles. Polymerization was carried out at a scan rate of 50 mV s⁻¹ in a potential window between -1.8 and 1.9 V with a step potential of 10 mV

the cyclic voltammogram obtained after the electropolymerization of the poly-EDA film, under different scan rates from 10 to 50 mV s⁻¹ in the presence of 5 mmol L⁻¹ K₄ [Fe(CN)₆]⁴⁻ / K₃ [Fe(CN)₆]³⁻ in 0.1 mol L⁻¹ KCl. An increase in redox current peaks was observed with the increase of scan rates, indicating that polymerized monomers on the electrode surface increased with the current density, reaching a plateau at 30 mV s⁻¹ (ESM Fig. S1b). A scan rate of 50 mV s⁻¹ was adopted for all subsequent experiments, due to it requiring less time to obtain film.

Electrochemical characterization of poly-EDA/CNT-COOH nanostructured film

The stability of the poly-EDA film was evaluated by subjecting the electrode to 25 consecutive cycles of CV in a potential ranging from -0.2 V to 0.6 V at a 50 mV s⁻¹ scan rate in the presence of 5 mmol L⁻¹ K₄ [Fe(CN)₆]⁴⁻ / K₃ [Fe(CN)₆]³⁻ in 0.1 mol L⁻¹ KCl. The coefficients of variation of the anodic and cathodic peaks were 0.01% to 0.1%, respectively, demonstrating that the poly-EDA film achieved excellent electrochemical stability, implying a further high reproducibility in analytical measurements [29]. Electrochemical diffusion processes on the poly-EDA film were also analyzed by CV in the presence of ferri/ferrocyanide as a redox probe (Fig. 2a). According to the amplitude of redox peaks, a linear increase of anodic and cathodic current peaks was observed, as a function of the square root of the scan rate with high correlation coefficients, found at 0.999 and 0.997, respectively, indicating a process controlled by diffusion (Fig. 2b). This behavior was also confirmed by the slope (*m*) of the logarithm of anodic and cathodic peaks of current versus the logarithm of scan rate (Fig. 2c). The *m* values were approximately 0.51 and 0.58, respectively, which means the system was mostly driven by diffusion, as opposed to a value close to 1.0 that would describe adsorptive behavior [30–32].

It is well-established that the binding of CNT-COOH to the sensor surface in an adsorptive way results in low reproducibility due to the leaching of nanomaterial during the analyses [33]. A covalent bond to the poly-EDA film can be achieved through an amide bond with the amino groups since the CNT used here was carboxyl-functionalized. Herein, the EDC/NHS chemistry was used for this purpose with the pre-activation of the CNT-COOH for subsequent bonding to the amino poly-EDA film. The CNT-COOH binding was confirmed by changes in the electrochemical profile with an increase in the electroactive area at the expense of capacitive and faradaic current. Previous studies using only the CNTs on electrode surfaces have shown CV results with a typical double-layer behavior [34, 35]. However, in this study, synergism between CNT-COOH and poly-EDA due to the strong linkage between two structures improved the conductivity with an increase of electron transfer rate, probably attributed to the non-

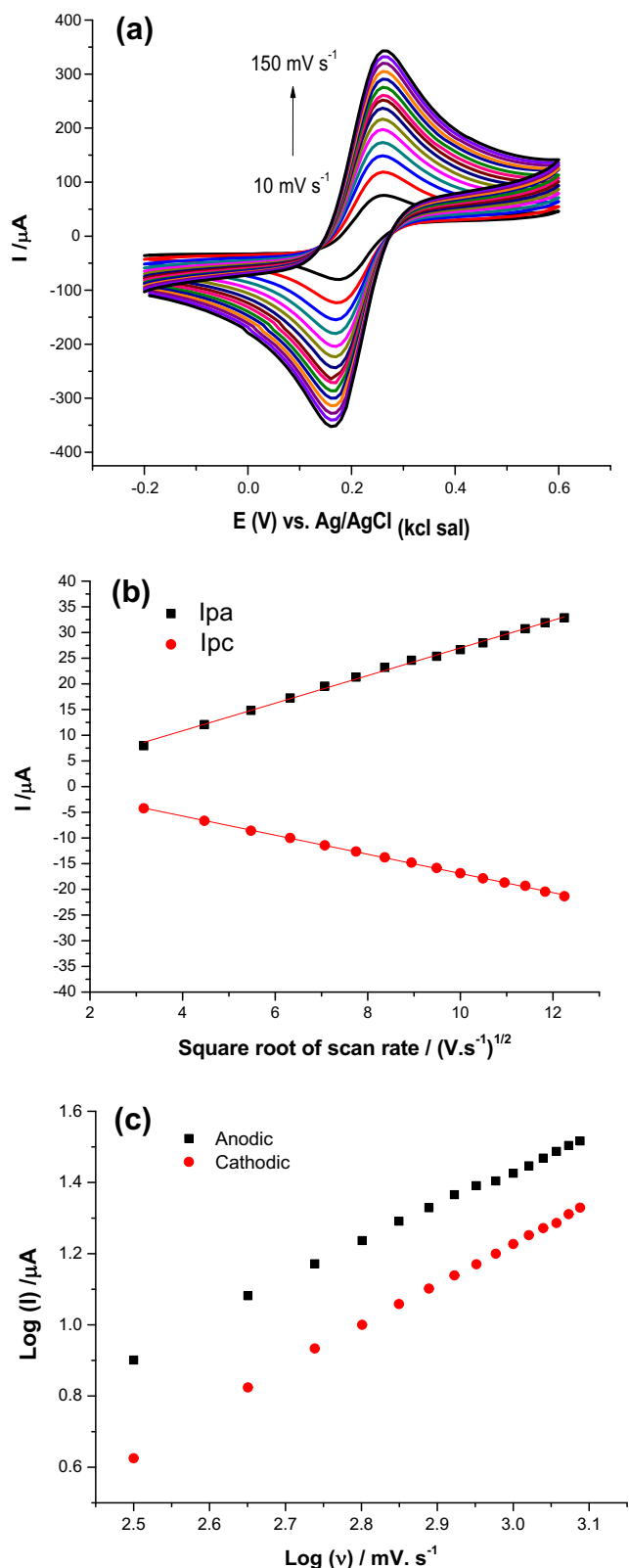


Fig. 2 (a) Cyclic voltammograms of poly-EDA film under different scanning rates of 10 → 150 mV s⁻¹ (10, 20, 30, 40, 50, 60, 70, 80, 90, 100, 110, 120, 130, 140 and 150 mV s⁻¹) in 5 mmol L⁻¹ of the K₄[Fe(CN)₆]⁴⁻/K₃[Fe(CN)₆]³⁻ in 0.1 M KCl. (b) Effect of the square root of the scan rate on the anodic and cathodic peaks. (c) Curves of the logarithm of the anodic and cathodic current peaks (*I*_{pa}, *I*_{pc}) versus the logarithm of the square root of scan rates

COOH promoting a high capacity to store charge [36, 37]. Based on the Randles–Sevcik equation [38], it is possible to quantify the contribution of nanomaterial by the increase of electroactive area after CNT-COOH linkage:

$$i_p = 0.4463nFAC\sqrt{\frac{nFD\nu}{RT}}$$

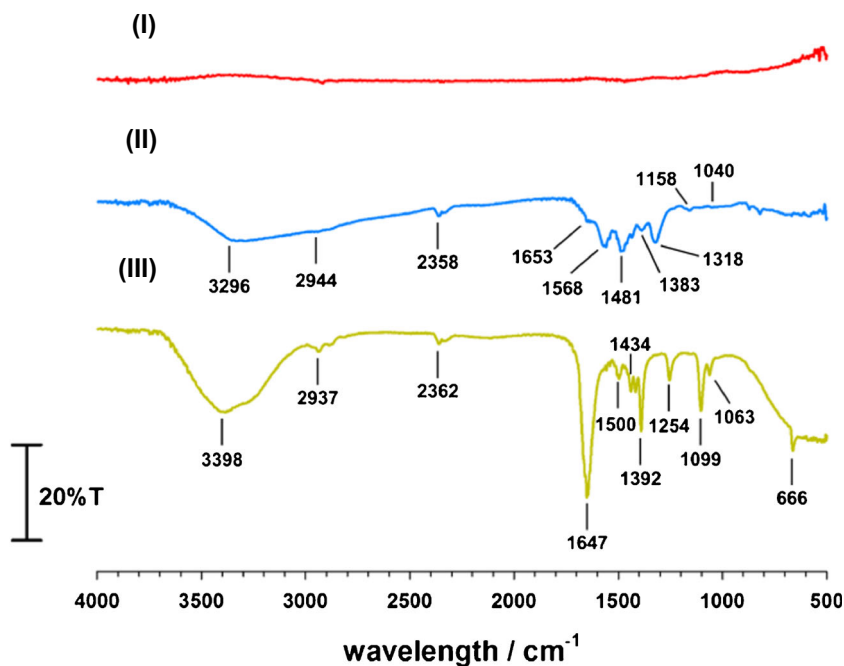
where *n* is the number of electrons, *F* is the Faraday constant, *A* is the area of the electrode, *C* is the concentration, *R* is the ideal gas constant, *T* is the temperature and *D* is the diffusion constant. An increase of approximately 1.8 times in the electroactive area was observed as compared to the poly-EDA, confirming that the electrosynthesized film behaved like the conducting polymer, simultaneously accelerating the transfer of electrons and increasing the charge storage, as confirmed by the increase of area approximately 4.5 times the bare electrode (ESM Fig. S1a). Here, the results show that the electrosynthesis of the poly-EDA film showed better electroactive conductivity compared to the polyethylenimine film obtained by drop-casting in previous studies [39]. It is believed that this can be attributed to the structure of the polymer formed, which appears to be linear and short-branched, which can promote greater electron transfer due to the structure of ionic bonds.

Given that the CNT-COOH amount bound to poly-EDA can affect the electroanalytical response by changing the electron transfer rate, studies were performed in different electrodes of poly-EDA modified by varying the concentration from 1 to 5 mg mL⁻¹ of previously dispersed CNT-COOH (ESM Fig. S2a). According to redox peaks of the cyclic voltammograms, the amount of CNT-COOH was limited to 4 mg mL⁻¹ when a plateau was reached (ESM Fig. S2b). This amount was limited by the availability of amine groups of the poly-EDA.

FTIR in the ATR mode is a very useful technique to analyze chemical surface modifications at nanoscale [40]. As can be observed in Fig. 3, there were evident differences between the bare gold electrode after deposition of the poly-EDA and after linking the CNT-COOH. As expected, the bare Au electrode showed no characteristic bands or peaks. The peaks around 2362 and 2358 cm⁻¹ can be explained by the CO₂ interference in the FTIR measurements [41]. There are some peaks that appear in both poly-EDA and poly-EDA/CNT-COOH that, obviously, are explained by the structure of the polymer: peaks around 2944 and 2937 cm⁻¹ can be attributed

branched structure of poly-EDA. Conductive polymers and CNT-COOH have shown excellent performance in the electron transfer, in addition to the high surface area of CNT-

Fig. 3 FTIR-ATR spectra in each step of the poly-EDA nanostructured film preparation: (I) bare EAU, (II) poly-EDA/EAU, (III) CNT-COOH/poly-EDA/EAU



to the axial deformation of C–H; the peaks around 1481 and 1500 cm^{-1} can be attributed to the angular deformation of C–H [27]; the peaks around 1383 and 1392 cm^{-1} can be attributed to the angular symmetric deformation of C–H; and the peaks in the region between 1200 and 1000 cm^{-1} (where the peaks 1158, 1040, 1099 and 1063 cm^{-1} can be found) can be attributed to the axial vibration of C–C [41]; however, it was specified that the 1063 cm^{-1} peak can also be attributed to the C–N stretching [27]. Then, there can be found a few changes from one spectrum to the other that can be explained by the reaction between the poly-EDA's amines and the carboxylic groups in the CNT-COOH forming amides (as schematized in Fig. 3): it seems that the band around 3296 cm^{-1} (in poly-EDA) can be attributed to the axial deformation of N–H. This band is large because it is a mixture between primary and secondary amines; then, after reaction (poly-EDA/CNT-COOH), the peak discretely shifted to the left (3398 cm^{-1}), and the band became narrower because there were more amides present and less primary amines. In the poly-EDA spectrum, there is a small peak (1653 cm^{-1}) that can be attributed to the axial deformation of N–H, another peak (1568 cm^{-1}) that can be attributed to the symmetric angular deformation of N–H, and the 1318 cm^{-1} peak that can be attributed to the amine's axial deformation of C–N [42]. Then, the poly-EDA/CNT-COOH spectrum showed a sharp peak at 1647 cm^{-1} that corresponded to the superimposition of the axial deformation of N–H along with the more intense axial deformation of the amide's C=O [43]. It is described that the C=O of the carboxylic acid is evident in the 1730–1700 cm^{-1} region, and the amide can appear in

the 1680–1630 cm^{-1} region; moreover, the small 1434 cm^{-1} peak can be attributed to the amide's axial deformation of C–N [41]. Finally, a few peaks were observed that can be attributed to the CNT-COOH, thus only appearing in the poly-EDA/CNT-COOH spectrum, namely, the 1254 cm^{-1} peak attributed to the scissoring vibration of the aromatic C–H and the 666 cm^{-1} attributed to a mono-substituted aromatic ring [44]. These results confirm the successful activation of the CNT-COOH anchoring to the amines in the poly-EDA film forming an amide linkage.

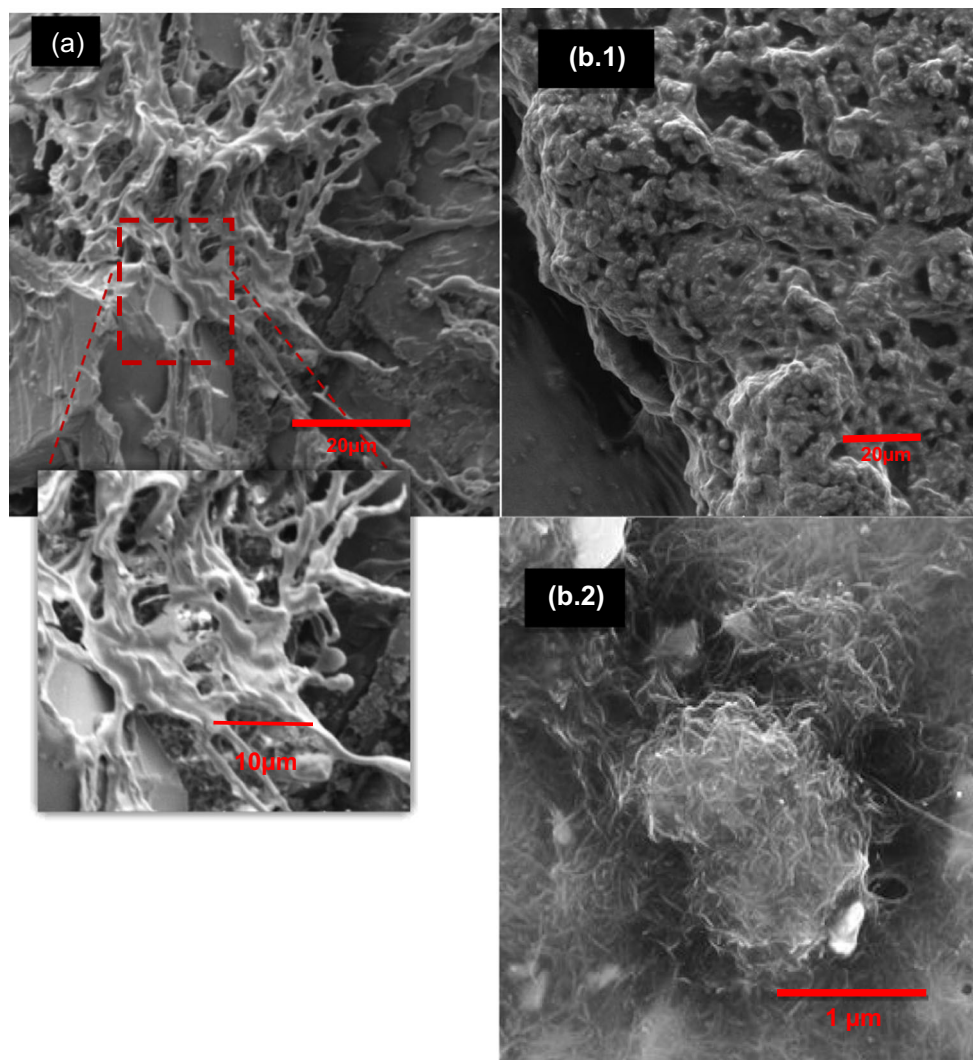
Morphological characterization

Scanning electron micrographs were obtained to study the conformational structures of poly-EDA and CNT-COOH. It is observed that the Au modified with poly-EDA polymer formed a polymer with a linear structure exhibiting a short-branched characteristic (Fig. 4a). The interaction of poly-EDA with CNT-COOH occurred in a really homogeneous way, with a homogeneous film covering all the CNT-COOH (Fig. 4b1 and b2). According to the CV, a significant improvement in the conductivity of the composite films was also observed as previously described in a polyethylenimine/CNT film [45].

Piezoelectric characterization

The QCM system is an excellent tool for studying rigid thin films [46], and was used to evaluate the stability and thickness of the poly-EDA film. Poly-EDA film was electropolymerized on the gold electrode of the quartz crystal,

Fig. 4 Scanning electron micrographs of the (a) poly-EDA and (b1 and b2) CNT-COOH/poly-EDA in different magnitudes



and frequency was taken in PBS buffer with pump flow stopped and compared to the initial time and after 24 h of sample monitoring. After 24 h of monitoring with a sampling frequency of 30 Hz, the frequency values were, respectively, 49.651 ± 5 Hz and 49.692 ± 6 Hz, showing no significant difference (paired *t* test, $p \gg 0.05$). This stability can be attributed to the formation of short and healthy chains, probably with more linear characteristics.

Taking into account that the thickness of the film can affect the analytical sensitivity due to modifying the electron transfer, thicknesses were studied using five electrodes in the QCM system described. Based on the frequency changes and density of the polymer, the thickness of the poly-EDA film ($t_{\text{poly-EDA}}$) could be calculated from the Δm , then using the poly-EDA density ($\rho_{\text{poly-EDA}}$) of 1.08 g mL^{-1} :

$$t_{\text{poly-EDA}} = \Delta m / \rho_{\text{poly-EDA}}$$

Thus, it was found that the average film thickness obtained was 104 ± 23 nm ($n = 5$), indicating a nanoscale film, as

expected. It was observed that the thickness of the poly-EDA films obtained by electropolymerization of triethanolamine increased proportionally to the electropolymerization time, obtaining an optimal at 13 min (0.1 M EDA) [47]; here, the film reached an average thickness of 100 nm in a shorter time, being also very homogeneous, as confirmed by symmetrical and regular peaks of the cyclic voltammograms. On the other hand, the EDA film was more quickly electropolymerized compared to triethanolamine, probably attributed to a shorter chain. Another advantage of electropolymerization compared to chemical synthesis and further drop-casting deposition is related to the reduction in the thickness, resulting in improved electron transfer.

Immobilization of anti-NS1 and blocking of the non-specific bindings

The immobilization of anti-NS1 antibodies was confirmed by the reduction of redox peaks and electroactive area due to the

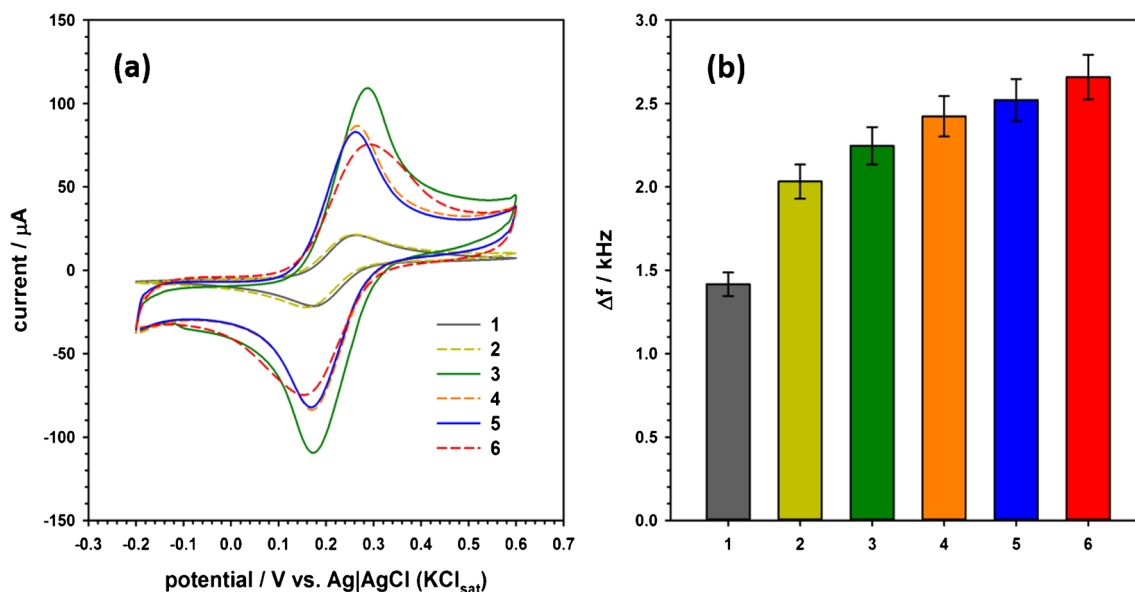


Fig. 5 Stepwise modifications in the immunosensor: (1) bare Eau, (2) poly-EDA/Eau, (3) CNT-COOH/poly-EDA/Eau, (4) anti-NS1/CNT-COOH/poly-EDA/Eau, (5) glycine/anti-NS1/CNT-COOH/poly-EDA/Eau and (6) NS1/anti-NS1/CNT-COOH/poly-EDA/Eau. In (a): cyclic

voltammograms obtained in the presence of $5 \text{ mmol L}^{-1} \text{K}_4[\text{Fe}(\text{CN})_6]^{4-} / \text{K}_3[\text{Fe}(\text{CN})_6]^{3-}$ in 0.1 M KCl ; and (b) Bar plot of the frequency changes in the QCM system measured in PBS

insulating nature of proteins, as seen in Fig. 5a, curve 4. In order to block nonspecific bindings, one aliquot ($2 \mu\text{L}$) of 50 mmol L^{-1} glycine solution was pipetted on the sensor surface. The decrease in redox peaks (curve 5) confirmed the blockage due to its similar insulating nature. Glycine is a very suitable block for biosensors since it has a low molecular weight with only one amino acid, not resulting in a change in the background current when compared to blocking with BSA or casein, commonly used in immunoassays.

Frequency changes in each step were also characterized by a piezoelectric system. Using the EDC/NHS chemistry, the effective anchoring of the CNT-COOH to the poly-EDA was verified by an increase in the shift frequency of the QCM system. Likewise, an increase in frequency shift was observed with successive steps, per the anti-NS1 antibody immobilization, as well as glycine blocking, and after NS1 antigen (100 ng mL^{-1}) response. In all these steps after the film, it is necessary to consider that the mass variation model does not correspond to a linear variation of mass on the electrode surface. It is mainly observed that when the sensor surface is covered by carbon nanotubes and followed by structured 3D proteins, deformations and changes in viscoelasticity occurring in the center of the electrode due to the movement of molecules on the sensor surface can affect the electric dipole of the quartz crystal [46]. Thus, although the model does not obey the Sauerbrey equation (1958) [48], changes in frequency by mass adsorption cannot be compared to the

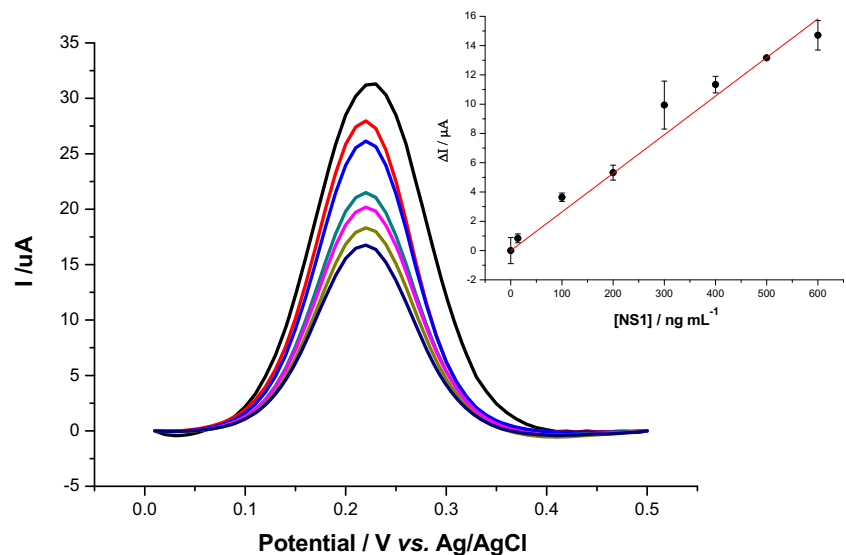
electrochemical technique, even though a gradual increase at each successive step is observed (Fig. 5b).

Analytical curve and interference study

Under optimal conditions, the immunosensor was evaluated in response to the NS1 in PBS, applying DPV as the electrochemical method. The current response was obtained by the difference of amplitude of the DPV cathodic peaks before and after incubation with NS1 prepared in the PBS. The calibration curve of the DPV current peaks was $\Delta i_p (\mu\text{A}) = (1.13 \pm 0.08) [\text{NS1}] (\mu\text{g mL}^{-1}) + (0.23 \pm 0.03)$ for three NS1 standard curves (values of the slope and intercept expressed as the adjusted data for the linear equation showed a coefficient of determination (R^2) of 0.9975, $p < 0.01$, $n = 7$) with a low relative error ($< 1\%$) (Fig. 6a and inset).

Analytical responses were also obtained with the recombinant NS1 spiked serum diluted 1:10 in PBS after successive incubations by DPV (ESM Fig. S3a). The curve obtained resulted in an R^2 of 0.9725 with a linear range between 20 and 800 ng mL^{-1} (ESM Fig. S3b). Based on the relative standard deviation (RSD) of the blank sample and slope of the analytical curve, the limit of detection according to the IUPAC was found at 6.2 ng mL^{-1} , comparable to that reported previously for labeled immunosensors [33, 49], however here with the advantage of practicality and fewer steps required,

Fig. 6 Immunosensor as response to NS1 diluted in PBS. Electrochemical DPV measurements obtained in the presence of $5 \text{ mmol L}^{-1} \text{ K}_4[\text{Fe}(\text{CN})_6]^{4-}/\text{K}_3[\text{Fe}(\text{CN})_6]^{3-}$ in 0.1 M KCl . Inset: analytical curve of the anodic peaks



due to the label-free detection. Impedimetric immunosensors for NS1 were also developed, showing a superior limit of detection [16, 50, 51] and a combination of impedimetric and lateral flow in an electrochemical immunosensor [17]; these works are presented in Table S1 (see ESM). Likewise, here, detection of the NS1 was demonstrated using a simpler effective electrochemical method. It has been reported that NS1 protein is found in circulation in serum at levels up to $50 \mu\text{g mL}^{-1}$, higher than that found in this study [52]. Thus, the designed immunosensor was able to detect the NS1 at the clinical level in serum, showing ability to distinguish NS1.

Further interference studies encompass typical agents that cause cross-reaction results, such as ascorbic acid present in the human blood, bovine serum albumin used as blocking agent, and human immunoglobulin G. According to the recovery factor (%), the average error found was less than 8% (ESM Table S2). It is noteworthy that the concentrations of studied interferents were higher than or similar to those found in human samples. These satisfactory results can be attributed to the effective glycine blockage that was carried out at a slightly acidic pH (5.5), below the isoelectric point of the glycine, making its amino groups available to block the CNT-COOH free remaining carboxyl moieties.

Real sample analysis

Regarding the selectivity to the NS1, this immunosensor was further investigated by subjecting it to real conditions with human serum samples of ZIKV and DENV from mono-infected patients and using a negative serum against both arboviruses as control. All the samples were previously checked according to the CDC's protocols, and

hemolyzed and hypercholesteremic samples were discarded since they can interfere with the analytical signal. DPV response curves of different electrodes after incubating with the ZIKV, DENV and control diluted in PBS are shown in Fig. 7a, b and c, respectively. According to Fig. 7d, serum samples diluted with PBS up to 1:50 showed significant differences between control and both infected individuals; however, NS1 was detected in ZIKV and DENV sera, as expected. Due to the high structural similarities between the viruses belonging to the *Flaviviridae* family, cross-reactivity is a key concern, primarily in the endemic regions where DENV and ZIKV are present, and the symptoms are also similar [53]. Additionally, there are many asymptomatic individuals. On the other hand, DENV/ZIKV co-infections may also occur [10].

Although RNA of the flavivirus is observed only in the urine of ZIKV-infected patients [10], recent studies have reported that the NS1 nonstructural protein occurs in ZIKV and DENV urine samples [8]. One advantage of urine for a rapid test is the noninvasive sample collection and higher sample volume. Here, a proof of concept was performed measuring NS1 in a spiked urine sample (Fig. 8a). The analytical performance of the immunosensor according to the DPV curves showed significant discrimination between control and NS1-spiked urine for NS1 concentrations up to 20 ng mL^{-1} , which was established as the cutoff (Fig. 8b). These results confirm the possibility of developing an immunosensor for ZIKV and DENV trials by detection of NS1, although more samples need to be tested.

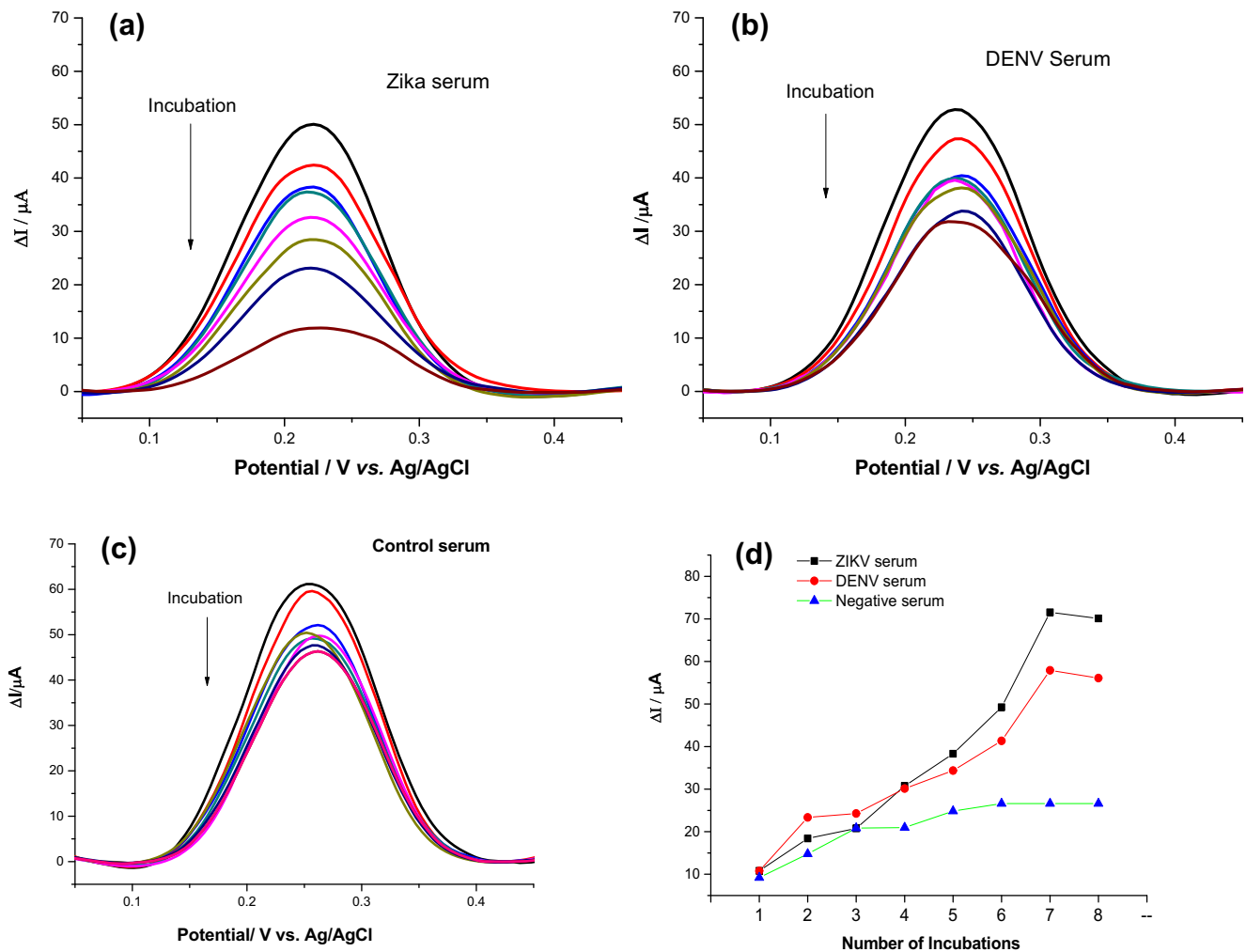


Fig. 7 DPV responses to real serum samples of (a) ZIKV-infected individuals, (b) DENV-infected individuals and (c) healthy individuals. (d) Calibration curves of anodic peaks of the ZIKV-infected, DENV-infected and healthy individuals

Repeatability and reproducibility

Repeatability and reproducibility are important analytical parameters in immunosensor performance. Herein, repeatability was obtained by analyzing ten successive measurements after incubating the electrode with sample serum spiked with 50 ng mL^{-1} of NS1, running an interval of 10 min for each one. The coefficient of variation for measurements of DPV, anodic and cathodic peaks of cyclic voltammograms and square-wave voltammograms are shown in bar plots in ESM Fig. S4a. The RSD values for I_{pa} and I_{pc} were highly similar, with good performance ($\text{RSD} < 5\%$). Reproducibility was assessed using the same techniques as repeatability on eight different electrodes (ESM Fig. S4b). For all the techniques, the RSD was about 5%, indicating the good selectivity of the designed immunosensor.

Conclusions

An immunosensor for NS1 protein detection was successfully developed for analyses in real samples of serum and showed possible used for urine samples. The electropolymerization method was used to synthesize a polymer film using cyclic voltammetry. Electrosynthesis compared with drop-casting enables the growth of films with more controlled thickness, chain lengths and electrochemical stability to result in better conductivity. In this study, poly-EDA film was obtained with nanoscale thickness, as confirmed by the QCM system. SEM images showed a short-branched polymer, implying an effective conductivity, and amine-rich moieties yielded profitable synergism between the CNT-COOH and poly-EDA by amide bonds, promoting a high electron transfer rate and good electrochemical stability. In

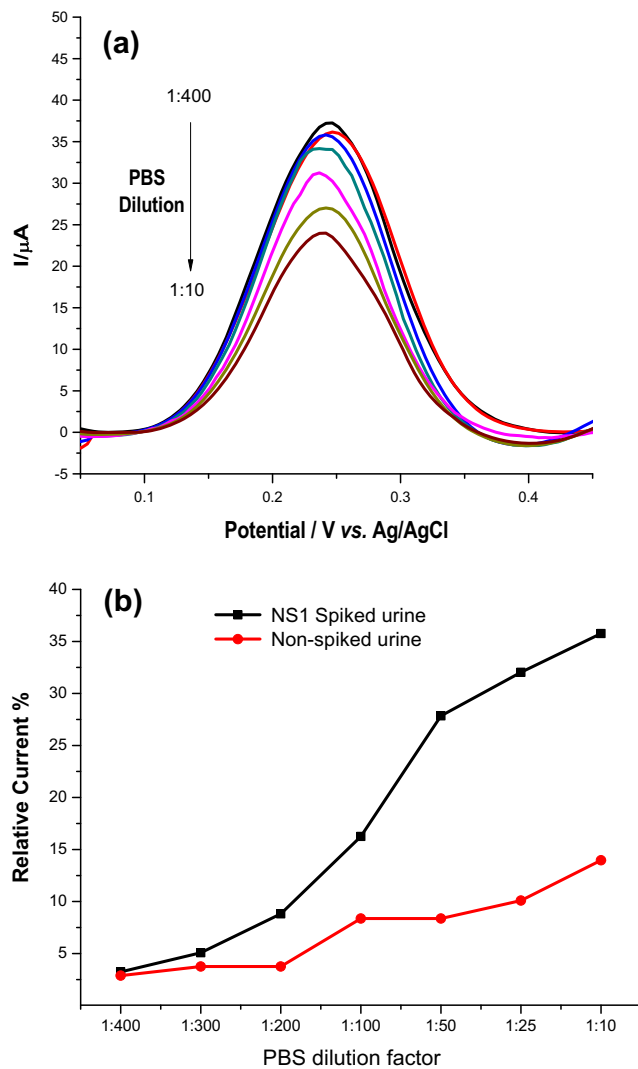


Fig. 8 (a) DPV curves in response to the NS1-spiked urine in different PBS dilutions, and (b) calibration curves of anodic peaks of the NS1-spiked and non-spiked urine samples

optimized conditions, this immunosensor was able to detect the NS1 with discrimination in serum and urine in complex medium, showing this proposed immunosensor has further potential for clinical analysis.

Supplementary Information The online version contains supplementary material available at <https://doi.org/10.1007/s00216-021-03449-7>.

Acknowledgments This work was supported by Research Brazilian Agency CNPq grant number 440605/2016-4 and CAPES from Brazil, Public Call to Prevent and Combat Zika Virus. Priscila Dias and Lorena Santos had scholarships from CAPES and FACEPE agencies, respectively, of Brazil.

Declarations

Conflict of interest The authors declare that they have no conflicts of interest.

Ethical approval This study was conducted in accordance with the Helsinki Declaration as revised in 2013. The serum samples used in this study are leftover samples from volunteers that signed the informed consent and authorized the use for research purposes. The study protocol was reviewed and approved by the local Ethics Committee on Human Research at the Instituto Aggeu Magalhães-Fundação Oswaldo Cruz (IAM-FIOCRUZ/Recife/Brazil) (approval ID 28309414.9.0000.5190).

References

- WHO. Dengue: causas, sintomas, tratamento e prevenção. 2019.
- Lim SP. Dengue drug discovery: Progress, challenges and outlook. *Antivir Res.* 2019;163:156–78.
- Bhatt S, Gething PW, Brady OJ, Messina JP, Farlow AW, Moyes CL, et al. The global distribution and burden of dengue. *Nature.* 2013;496(7446):504–7.
- Alcalá AC, Palomares LA, Ludert JE. Secretion of Nonstructural Protein 1 of Dengue Virus from Infected Mosquito Cells: Facts and Speculations. *J Virol [Internet].* 2018; 92(14): e00275–18.
- Ahmed NH, Broor S. Comparison of NS1 antigen detection ELISA, real time RT-PCR and virus isolation for rapid diagnosis of dengue infection in acute phase. *J Vector Borne Dis.* 2014;51(3): 194–9.
- Lim JK, Lee Y-S, Wilder-Smith A, Thiry G, Mahoney R, Yoon I-K. Points for consideration for dengue vaccine introduction – recommendations by the dengue vaccine initiative. *Expert Rev Vaccines.* 2016;15(4):529–38.
- Lustig Y, Koren R, Biber A, Zuckerman N, Mendelson E, Schwartz E. Screening and exclusion of Zika virus infection in travellers by an NS1-based ELISA and qRT-PCR. *Clin Microbiol Infect.* 2020;26(12):1687.e7–1687.e11.
- Korhonen EM, Huhtamo E, Virtala AMK, Kantele A, Vapalahti O. Approach to non-invasive sampling in dengue diagnostics: exploring virus and NS1 antigen detection in saliva and urine of travelers with dengue. *J Clin Virol.* 2014;61(3):353–8.
- Sharma V, Sharma M, Dhull D, Sharma Y, Kaushik S, Kaushik S. Zika virus: an emerging challenge to public health worldwide. *Can J Microbiol.* 2020;66(2):87–98.
- Bosch I, De Puig H, Hiley M, Carré-Camps M, Perdomo-Celis F, Narváez CF, et al. Rapid antigen tests for dengue virus serotypes and zika virus in patient serum. *Sci Transl Med [Internet].* 2017 Sep 27 [cited 2021 Jan 25];9(409). Available from: /pmc/articles/PMC6612058/?report=abstract.
- Musso D, Ko AI, Baud D. Zika virus infection — after the pandemic. *N Engl J Med.* 2019;381(15):1444–57.
- Mishra N, Caciula A, Price A, Thakkar R, Ng J, Chauhan L, et al. Diagnosis of Zika virus infection by peptide array and ELISA. *MBio.* 2018;9(2):1–16.
- Borges ED, Vireque AA, Berteli TS, Ferreira CR, Silva AS, Navarro PA. An update on the aspects of Zika virus infection on male reproductive system. Vol. 36, *Journal of Assisted Reproduction and Genetics.* Springer New York LLC; 2019. p. 1339–49.
- Camara AR, Gouvêa PMP, Dias ACMS, Braga AMB, Dutra RF, De Araujo RE, et al. Dengue immunoassay with an LSPR fiber optic sensor. *Opt Express.* 2013;21(22).
- Darwish NT, Sekaran SD, Alias Y, Khor SM. Immunofluorescence-based biosensor for the determination of dengue virus NS1 in clinical samples. *J Pharm Biomed Anal.* 2018;149:591–602.

16. Cecchetto J, Carvalho FC, Santos A, Fernandes FCB, Bueno PR. An impedimetric biosensor to test neat serum for dengue diagnosis. Vol. 213, *Sensors and Actuators B: Chemical*. 2015.
17. Sinawang PD, Rai V, Ionescu RE, Marks RS. Electrochemical lateral flow immunosensor for detection and quantification of dengue NS1 protein. *Biosens Bioelectron*. 2016;77:400–8.
18. Dhal A, Kalyani T, Ghorai S, Sahu NK, Jana SK. Recent development of electrochemical immunosensor for the diagnosis of dengue virus NS1 protein: A review. *Sensors Int*. 2020;1:100030.
19. Bajpai OP, Kumar S, Bhandari S, Dhar A, Khastgir D, Chattopadhyay S. Electrolyte and current density determines the fate of electrodeposited polythiophene from waveguide to photovoltaics. *Sol Energy Mater Sol Cells*. 2018;183:107–19.
20. Watanabe T, Ohira M, Koizumi Y, Nishiyama H, Tomita I, Inagi S. In-plane growth of poly(3,4-ethylenedioxythiophene) films on a substrate surface by bipolar Electropolymerization. *ACS Macro Lett* 2018;7(5):551–5.
21. Ferreira PAB, Araujo MCM, Prado CM, de Lima RA, Rodríguez BAG, Dutra RF. An ultrasensitive cystatin C renal failure immunosensor based on a PPy/CNT electrochemical capacitor grafted on interdigitated electrode. *Colloids Surfaces B Biointerfaces* 2020;189.
22. Salavagione HJ, Diez-Pascual AM, Lázaro E, Vera S, Gómez-Fatou MA. Chemical sensors based on polymer composites with carbon nanotubes and graphene: the role of the polymer. *J Mater Chem A*. 2014;2(35):14289–328.
23. Mangione MI, Spanevello RA, Minudri D, Cavallo P, Otero L, Fungo F. Electrochemical films deposition and electro-optical properties of bis-carbazol-triphenylamine end-capped dendrimeric polymers. *Electrochim Acta*. 2018;263:585–95.
24. Duan S, Yue R, Huang Y. Polyethylenimine-carbon nanotubes composite as an electrochemical sensing platform for silver nanoparticles. *Talanta*. 2016;160:607–13.
25. Mattos AB, Freitas TA, Kubota LT, Dutra RF. An o-aminobenzoic acid film-based immunoelectrode for detection of the cardiac troponin T in human serum. *Biochem Eng J*. 2013;71.
26. Dias ACMS, Gomes-Filho SLR, Silva MMS, Dutra RF. A sensor tip based on carbon nanotube-ink printed electrode for the dengue virus NS1 protein. *Biosens Bioelectron* [Internet]. 2013 15 [cited 2017 Dec 11];44:216–21. Available from: <https://www.sciencedirect.com/science/article/pii/S0956566312008895>
27. Lakard S, Herlem G, Lakard B, Fahys B. Theoretical study of the vibrational spectra of polyethylenimine and polypropylenimine. *J Mol Struct {THEOCHEM}*. 2004;685(1–3):83–7.
28. Patois T, Lakard B, Martin N, Fievet P. Effect of various parameters on the conductivity of free standing electrosynthesized polypyrrole films. *Synth Met*. 2010;160(19–20):2180–5.
29. da Fonseca AR, Franco DL, Cordeiro MT, de Oliveira EM, Fireman Dutra RA, Del Pilar Taboada Sotomayor M. Novel electrochemical genosensor for Zika virus based on a poly-(3-amino-4-hydroxybenzoic acid)-modified pencil carbon graphite electrode. *Sensors Actuators, B Chem*. 2019;296.
30. Batchelor-McAuley C, Goncalves LM, Xiong L, Barros AA, Compton RG. Controlling voltammetric responses by electrode modification; using adsorbed acetone to switch graphite surfaces between adsorptive and diffusive modes. *Chem Commun*. 2010;46(47):9037–9.
31. Gonçalves LM, Batchelor-McAuley C, Barros AA, Compton RG. Electrochemical oxidation of adenine: A mixed adsorption and diffusion response on an edge-plane pyrolytic graphite electrode. *J Phys Chem C*. 2010;114(33):14213–9.
32. Trindade EKG, Silva BVM, Dutra RF. A probeless and label-free electrochemical immunosensor for cystatin C detection based on ferrocene functionalized-graphene platform. *Biosens Bioelectron* 2019;138.
33. Silva MMS, Dias ACMS, Cordeiro MT, Marques E, Goulart MOF, Dutra RF. A thiophene-modified screen printed electrode for detection of dengue virus NS1 protein. *Talanta*. 2014;128:505–10.
34. Chen JH, Li WZ, Wang DZ, Yang SX, Wen JG, Ren ZF. Electrochemical characterization of carbon nanotubes as electrode in electrochemical double-layer capacitors. *Carbon N Y*. 2002;40(8):1193–7.
35. Hoefler M, Bandaru PR. Determination and enhancement of the capacitance contributions in carbon nanotube based electrode systems. 2009 [cited 2018 Dec 12]; Available from: http://maecourses.ucsd.edu/groups/bandaru/Publications_files/APL_paper_capacitance_contributions.pdf
36. Barbosa S, Gozze AB, Lima NF, Batista CL, da Bastos MS, Nicolette VC, et al. Epidemiology of Disappearing *Plasmodium vivax* Malaria: A Case Study in Rural Amazonia. Rodrigues MM, editor. *PLoS Negl Trop Dis* [Internet]. 2014 28 [cited 2019 Oct 9];8(8):e3109. Available from: <http://dx.plos.org/10.1371/journal.pntd.0003109>
37. Song H, Li T, Han Y, Wang Y, Zhang C, Wang Q. Optimizing the polymerization conditions of conductive polypyrrole. *J Photopolym Sci Technol*. 2016;29(6):803–8.
38. Mundinamani SP, Rabinal MK. Cyclic Voltammetric Studies on the Role of Electrode, Electrode Surface Modification and Electrolyte Solution of an Electrochemical Cell [Internet]. Vol. 7, *IOSR Journal of Applied Chemistry (IOSR-JAC)*. 2014 [cited 2019 Jun 2]. Available from: www.iosrjournals.orgwww.iosrjournals.org
39. Gomes-Filho SLR, Dias ACMS, Silva MMS, Silva BVM, Dutra RF. A carbon nanotube-based electrochemical immunosensor for cardiac troponin T. *Microchem J* [Internet]. 2013 Jul [cited 2018 May 16];109:10–5. Available from: <http://linkinghub.elsevier.com/retrieve/pii/S0026265X12001518>
40. Trindade EKG, Dutra RF. A label-free and reagentless immunoelectrode for antibodies against hepatitis B core antigen (anti-HBc) detection. *Colloids Surfaces B Biointerfaces* [Internet]. 2018 Dec 1 [cited 2019 mar 21];172:272–9. Available from: <http://www.ncbi.nlm.nih.gov/pubmed/30173094>
41. Silverstein RM, Webster FX, Kiemle DJ, Bryce DL. *Spectrometric Identification of Organic Compounds*. Wiley; 2014.
42. Rodríguez MC, Rubianes MD, Rivas GA. Highly selective determination of dopamine in the presence of ascorbic acid and serotonin at glassy carbon electrodes modified with carbon nanotubes dispersed in polyethylenimine. *J Nanosci Nanotechnol*. 2008;8(11):6003–9.
43. Murugan E, RC Akshata, Stephy A. Electrochemical sensing of anti-cancer drug (capecitabine) by GC-MWCNT-PAMAM (G3)-AuNps electrode. *Adv Mater Proc* 2017;2(3):176–183.
44. Pavia DL, Lampman GM, Kriz GS, Vyvyan JR. *Introdução à Espectroscopia*. Cengage; 2015.
45. Zou G, Jain M, Yang H, Zhang Y, Williams D, Jia Q. Recyclable and electrically conducting carbon nanotube composite films. *Nanoscale*. 2010;2(3):418–22.
46. Chen Q, Xu S, Liu Q, Masliyah J, Xu Z. QCM-D study of nanoparticle interactions. Vol. 233, *Advances in Colloid and Interface Science*. Elsevier B.V.; 2016. p. 94–114.
47. Rivera-Nieblas JO, Alvarado-Rivera J, Acosta-Enríquez MC, Ochoa-Landin R, Espinoza-Beltrán FJ, Apolinar-Irbe A, et al. resistance and resistivities of pbs thin films using polyethylenimine by chemical bath deposition. Vol. 10, *Chalcogenide Letters*. 2013.
48. Sauerbrey G. Verwendung von Schwingquarzen zur Wägung dünner Schichten und zur Mikrowägung. *Zeitschrift für Phys*. 1959;155(2):206–22.
49. Parkash O, Yean C, Shueb R. Screen Printed Carbon Electrode Based Electrochemical Immunosensor for the Detection of Dengue NS1 Antigen. *Diagnostics* [Internet]. 2014 Nov 20 [cited 2021 Feb 2];4(4):165–80. Available from: <http://www.mdpi.com/2075-4418/4/4/165>

50. Nawaz MH, Hayat A, Catanante G, Latif U, Marty JL. Development of a portable and disposable NS1 based electrochemical immunosensor for early diagnosis of dengue virus. *Anal Chim Acta* [Internet]. 2018 Oct 5 [cited 2021 Feb 4];1026:1–7. Available from: <https://doi.org/10.1016/j.aca.2018.04.032>
51. Guzman MG, Harris E. *Dengue Lancet*. 2015;385(9966):453–65.
52. Muller DA, Young PR. The flavivirus NS1 protein: Molecular and structural biology, immunology, role in pathogenesis and application as a diagnostic biomarker. [Internet]. Vol. 98, *Antiviral Research*. Elsevier B.V.; 2013 [cited 2021 Jan 24]. p. 192–208. Available from: <https://pubmed.ncbi.nlm.nih.gov/23523765/>
53. Gulland A. Zika virus is a global public health emergency, declares WHO. *BMJ*. 2016;352(February):i657.

Publisher's note Springer Nature remains neutral with regard to jurisdictional claims in published maps and institutional affiliations.